Contents lists available at ScienceDirect

Applied Thermal Engineering

journal homepage: www.elsevier.com/locate/apthermeng

Research Paper

A novel direct liquid cooling strategy for electric vehicles focused on pouch type battery cells

M. Larrañaga-Ezeiza [a,b,*], G. Vertiz [a], P.F. Arroiabe [b], M. Martinez-Agirre [b], J. Berasategi [b]

[a] CIDETEC, Basque Research and Technology Alliance (BRTA), Po. Miramón 196, 20014 Donostia-San Sebastián, Spain
[b] Mechanical and Industrial Production Department, Faculty of Engineering, Mondragon Unibersitatea, Loramendi 4, E-20500 Arrasate-Mondragón, Spain

ARTICLE INFO

Keywords:
Electric vehicles
Lithium-ion
Direct liquid cooling
Thermal management
Pouch cells
Partial cooling strategy

ABSTRACT

In this work, a novel direct liquid cooling strategy for a large-scale lithium-ion pouch type cell is proposed to control the cell working temperature within the optimum range of performance and safety. With a modular design to reduce the weight impact of the fluid, the novelty of the strategy consists in directly cooling the surface of the battery cell instead of immersing the battery system in the cooling fluid. To evaluate the feasibility of the proposed strategy, a sub-system level comparison with the indirect liquid cooling strategy was developed based on the pumping power consumption criterion. Both strategies were subjected to 1C pulse tests and real driving cycles. At 1C pulse tests, the mean cell temperature was 6.4 °C lower, and the thermal heterogeneity decreased from 5.7 °C to 0.4 °C. The real driving cycle results showed the faster response of the direct liquid cooling strategy, which instantaneously reduced the cell temperature to the cooling setpoint after a semi-fast charge in each driving cycle. This study highlights the higher performance of the proposed strategy, which delivers more accurate thermal management without increasing power consumption. Thus, the proposed strategy provides a feasible high-performance solution for high-capacity Li-ion based electric vehicle applications.

1. Introduction

Electric mobility is key to reducing CO_2 emissions from highly populated areas. One further advantage is that this strategy can also contribute to the development of an interactive energy network. Many countries have already announced 100 % zero-emission targets defining a 2050 deadline [1]. These types of initiatives are driving the growth of electric vehicles on the world's roads and have created a dynamic market that demands high performance vehicles. These new vehicles require increased energy, power density, safety, battery cycle life, and charging velocity. The requirements are directly linked with the performance of the battery system and define one of greatest challenges for electric vehicle development: how to maintain the maximum performance and safety of the battery system while demanding maximum working conditions.

Batteries based on Lithium-ion chemistry are the most widely used energy storage components in the HEV/EV sector due to their technical characteristics. Based on the energy density, these batteries are capable of accumulating between 50 and 260 gravimetric Wh, have a high discharge capacity (1–30C), are more durable (300–7000 cycles >80% DoD), and require less maintenance [2]. Lithium-ion batteries can work with a percentage of <5% auto discharge/month and their performance has a low degradation rate, as long as the working temperature is appropriate.

The performance of this technology is highly influenced by temperature and working outside the optimal operating ranges can cause safety issues and reduce cell life by >50% [3]. The optimum temperature operating range is between 15 and 40 °C, and constitutes a working range where the relationship between the performance and the safety of the battery cell is optimum [4,5,6]. Working at temperatures below the defined range (<15 °C), considerably decreases the battery cell capacity [7]. Low temperatures increase the density of the electrolyte and complicate the transition of ions between the cathode (positive electrode) and anode (negative electrode). In addition, the inner resistance of the cell and dendritic growth (Lithium Plating) increase, which negatively influence the capacity of the cell [8,9,10]. Working above the defined temperature range (>40 °C) affects the performance of the cells to a lesser extent. However, it is more dangerous because of the risk of initiating Thermal Runaway (TRA), an exothermic reaction that accelerates with the increase of temperature. This reaction causes an irreparable damage to the battery system and has critical safety implications for occupants of the vehicle [11]. Finally, it should be noted that even if the battery cell mean temperature is within the optimal temperature

* Corresponding author.
E-mail address: mlarranaga@cidetec.es (M. Larrañaga-Ezeiza).

https://doi.org/10.1016/j.applthermaleng.2022.118869
Received 15 March 2022; Received in revised form 24 May 2022; Accepted 14 June 2022

Nomenclature

Superscripts

C	battery cell capacity (Ah)
c_p	specific heat capacity (kJ/kgK)
I	current (A)
m	mass (kg)
$\dot{m}$	mass flow rate (kg/min)
P_h	hydraulic power (W)
ΔP	pressure difference (kPa)
Q_c	calorific power (W)
Q_f	heat absorbed by the fluid (W)
T	temperature (°C)
ΔT	temperature difference (°C)
V	voltage (V)
V	volumetric flow rate (L/min)

Subscripts

amb	ambient
c	cell
cc	charge current
c,t	cell to tab
dc	discharge current
f	fluid
in	fluid inlet temperature
max	maximum
mean	average value
min	minimum
n	nominal
ss	subsystem
t	tab

Acronyms

AM	additive manufacturing
BMS	battery management system
BTMS	battery thermal management system
CAD	computer-aided design
CAN	controller area network
COP	coefficient of performance
DLC	direct liquid cooling
DoD	battery depth of discharge
ECM	equivalent circuit model
EV	electric vehicle
FDM	fused deposition modelling
HEV	hybrid electric vehicle
HP	heap pipe
ILC	indirect liquid cooling
NMC	nickel manganese cobalt
OCV	battery open circuit voltage
PCM	phase change material
SOC	battery state of charge
TEC	thermoelectric cooler
TIM	thermal interface material
TRA	thermal runaway

range, thermal heterogeneities can affect cell performance. Thus, a cell level temperature distribution below 5 °C is recommended [12].

Considering the influence of the working temperature on the safety and performance of the battery system, thermal management is becoming increasingly important [13,14]. In this context, numerous studies have been conducted analysing different cooling technologies to develop thermal control of the battery system. These strategies are generally classified as air cooling, Indirect Liquid Cooling (ILC), Phase Change Materials (PCM), Heat Pipes (HP), and Thermoelectric coolers (TEC) [15]. The low cost of the application and the capacity of the fluid to directly contact the heat generation component (battery cell), makes air cooling an attractive solution. However, the low heat absorption capacity of the air makes this strategy unsuitable for current EV working requirements [16]. PCM cooling provides a passive control using the latent heat of the phase change to remove the heat rejected from the cells [17]. Nevertheless, with high power demands, a secondary cooling strategy is required to remove all the heat absorbed without saturating the material [18]. HP technology is highly effective at transferring heat from the batteries to the cooling area due to the characteristics of the fluid used in the system. However, in addition to the need for a secondary cooling system to remove the heat absorbed, this technology involves an increment of volume and cost that negatively influences the feasibility [19]. Finally, despite the theoretical efficiency of TEC technology, the cost of the materials results in a low coefficient of performance (COP). Therefore, it is not competitive at present [18].

Indirect liquid cooling is the strategy that predominates the thermal management of the electric vehicle sector. Thermal conductivity and the heat capacity of the implemented fluids (usually water glycol or refrigerant) enable the strategy to meet high heat generation demands [20,21]. However, these fluids are electrically conductive, which prevents contact between the heat generation point (battery cell) and the cooling fluid. Therefore, it is necessary to implement additional elements to electrically isolate both parts and thus, develop indirect contact cooling. This characteristic negatively influences the cooling efficiency of the strategy and adds thermal inertias to the system [22,23]. Furthermore, the aforementioned cooling and insulation components increase the weight and cost of the overall system, rendering it ineffective for the demands of the electric vehicle sector.

Considering the drawbacks of indirect liquid cooling, a cooling strategy based on direct liquid cooling has been the subject of many studies in recent years. [24-28]. This strategy uses dielectric fluids which have negligible electrical conductivity due to their high dielectric strength. This enables direct contact between the cooling liquid and the battery cell which increases the cooling capacity of the strategy and addresses the disadvantages of indirect liquid cooling. The most widely used cooling concept of this strategy is immersion cooling, which is based on covering the battery system with dielectric fluid to improve the cooling efficiency. Recent studies have demonstrated experimentally and numerically the higher thermal performance of direct liquid immersion cooling strategy. Following the work developed by Pulugundla et al. [29], Dubey et al. [30] developed a module level numerical study, in which the performance of direct and indirect cooling strategies were compared at different C-rate levels (current values with respect to its nominal capacity) in a battery module made by 21,700 cylindrical cells. The authors concluded that direct liquid immersion cooling presented significantly better battery cell temperature values than the ILC strategy, especially at high C-rates. Furthermore, authors observed that the pressure drop was 15–25 times lower for the DLC strategy, making it even more interesting. Using 2.75 Ah NMC811 cylindrical battery cells, Wu et al. [31] designed and fabricated an 8.32 kWh battery system based on direct liquid immersion cooling. Testing the battery system at 0.5C charge and 1C discharge rates, temperature differences of 4.9 °C and 8.8 °C were observed, respectively, maintaining maximum temperatures within the optimum working temperature range. However, the mass and volume of the DLC strategy were 1.1 and 1.5 times that of the indirect system. Finally, Patil et al. [32] developed a numerical and experimental study to analyse the performance of different cooling methods, including a mixed strategy based on direct liquid immersion cooling and air cooling. Defining a battery module of 50 V with 14 pouch type cells of 20 Ah, the authors examined the performance of the

selected strategy at different discharge rates (1–5C). In line with the other mentioned studies, the authors demonstrated the capacity of the selected strategy to maintain the battery module temperature within the optimum range (<40 °C) at high discharge rates, reducing the maximum temperatures of the battery module by 9.3 % compared to indirect liquid cooling. Interestingly, although the pumping power analysis of the DLC strategy was included in the study. Nevertheless, this variable was not incorporated in the comparison.

Overall, these studies indicate that the direct liquid immersion cooling strategy presents higher thermal performance than conventional strategies. In contrast, the higher viscosity of some dielectric fluids increases the power consumption of the system, and the quantity of the fluid needed to develop the strategy increments the overall weight of the battery pack. To date, there have been few experimental studies which considered both parameters in the comparison, and the pouch type are in the minority, where the scale up to a module level becomes more complicated. Furthermore, most of the research did not compare the thermal response under real working transient conditions.

Therefore, the present work proposes a comparison between a conventional ILC method, and a novel strategy based on a partial direct liquid cooling for a large-scale lithium-ion 60 Ah NMC pouch type cell. Originally, a direct experimental comparison based on the pumping power consumption criterion is proposed to contrast, under the same working conditions, the performance of the proposed strategy with the indirect liquid cooling strategy. Furthermore, to reduce the impact on weight increment, the proposed strategy focuses on the cooling effect on one area of the battery cell, instead of immersing the battery system in the cooling fluid. This approach is enabled by a specific prototype design that integrates several channels for the fluid, which is also modular to extend it to module level. For studying the influence of the cooling strategy at real working conditions, the thermal response time of the battery system under transient semi-fast charges was also examined.

2. System description

In this work, a large scale 60 Ah NMC pouch type battery cell was selected to develop the analysis of different cooling strategies. The general characteristics are depicted on Table 1. This type of battery cell has a flexible structure that allows it to fit easily in the available space and reduce the weight impact on the battery system. This characteristic improves the packaging efficiency and increases energy density in terms of optimization.

It is crucial to understand the operational heat generation of the battery cell to design an effective and efficient thermal management strategy. Therefore, the selected battery cell was tested in charge and discharge processes at different C-rate values in a THT EV + ARC calorimeter. All tests were initialized at 23 °C, and in a 0–100% SOC level, the calorific power results are shown in Fig. 1. These values were calculated by equation $Q_c = mc_p dT/dt$. Where Q_c was the calorific power (W), m was the cell mass, c_p was the specific heat of the battery cell (J/kgK), and dT/dt was the temperature variation over time (K/s). As it is presented, at 0–100% SOC the mean heat generation values at discharging process are higher than in the charging process. This characteristic is caused by the increase of the internal resistance of the cell when discharging above 90 % DoD and by the part of the entropic generation where endothermic behaviour is present in the charging process. It is therefore recommended not to work at deep SOC levels.

Table 1
Reference battery cell general characteristics.

Parameter	Value
Nominal voltage (V_n)	3.68 V
Minimum voltage (V_{min})	2.7 V
Maximum voltage (V_{max})	4.2 V
Nominal capacity (C_n)	60 Ah
Charging current (I_{cc})	120 A
Discharging current (I_{dc})	180 A
Charging temperature (T_{cc})	10/35 °C
Discharging temperature (T_{dc})	−20/50 °C
Electrolyte	Carbonated based
Anode material	Graphite
Cathode material	$LiNiMnCoO_2$
Dimensions	226 × 227 × 12 mm^3
Mass	1.140 kg
Tab material	Positive: Aluminium Negative: Cooper

An innovative thermal management strategy is proposed in this work, considering the battery cell referenced in Table 1. This strategy is based on direct liquid cooling and enables the contact between the refrigeration fluid and the battery cell. A cell level prototype based on direct liquid cooling was developed and experimentally tested to analyse the performance of the proposed strategy. Furthermore, to validate the proposed strategies feasibility, a comparison with the indirect liquid cooling strategy was developed, the reference strategy in the HEV/EV field.

2.1. ILC strategy description

To develop this comparison, a specific battery system based on indirect liquid cooling was selected. This battery system is based on a 2-module sub-system and is used in electric bus applications. Each of the modules has 24 pouch type battery cells of 60 Ah and the cooling strategy uses a cold plate as a cooling component to control the thermal behaviour of the battery system from the bottom, asFig. 2c shows. This type of strategy uses electrically conductive fluids (Water glycol 50/50 %v), therefore, the battery cell has to be insulated defining an indirect liquid cooling. As Fig. 2a shows, to enable the effect of the cooling strategy ensuring the insulation of the battery system, different components were defined between the battery cell and the cold plate. For each battery cell, an aluminium heatsink was implemented between the cell surface and the cold plate to develop contact between them, and thermal interface materials (TIM) were implemented to improve the contact between the heatsinks and the cold plate and insulate electrically the battery cell. This cell level structure was scaled up to a module level defining a framed linear pattern of the cell assembly. To equal the thermal behaviour of both modules, a specific design was implemented on the cold plate (Fig. 2b) with a proportional distribution of cooling channels per module to ensure similar heat transference on both contact surfaces.

2.2. Proposed DLC strategy description

The strategy proposed has two main differences compared to the indirect liquid cooling and the most known direct liquid cooling strategy based on immersion cooling. Compared to indirect liquid cooling, the direct liquid cooling strategy uses dielectric fluids, fluids with high dielectric strength that enables direct contact between the refrigeration fluid and the battery cell. Characteristic that reduces the thermal resistance between the refrigeration fluid and the battery cell. On the other hand, comparing with direct liquid immersion cooling, this strategy proposes a cooling focused on a specific area, the surface of the battery cell. This difference reduces the weight of the fluid needed and improves the volumetric energy density of the system.

The proposed direct liquid cooling strategy was developed using as a starting point the reference battery cell. Specifically, a lithium-ion 60 Ah NMC pouch type battery cell with the characteristics presented on Table 1. As it is mentioned, pouch type cells are flexible. Therefore, to rigidify the cell a prismatization component was designed as a prototype baseline. Apart from having a structural function, on the internal surface of this component, where the battery cell relies, some channels were defined creating a space to enable the circulation of the cooling fluid. This space enables the direct contact between the battery cell and the fluid, thus, it was designed as a cooling channel to provide the optimum

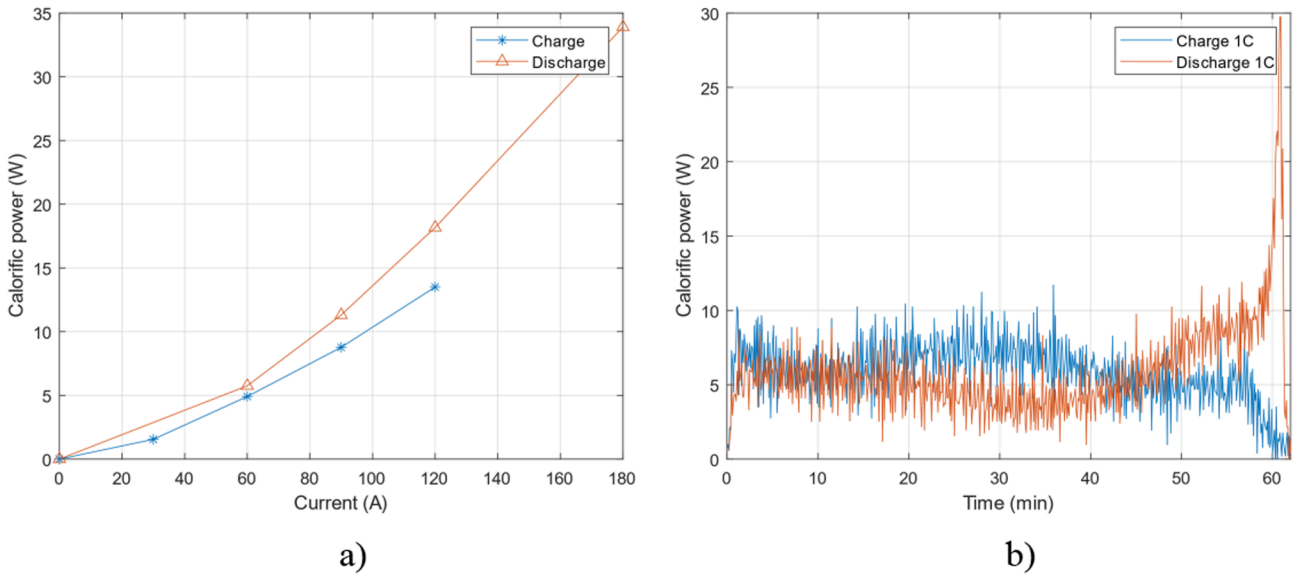

Fig. 1. Selected battery cell 0–100% SOC level charge and discharge heat generation testing results at (a) different C-rates values and (b) the transitory information of 1C tests.

refrigeration effect. To define this geometry, different designs were analysed and the one that presents the best ratio between thermal control and pressure drop was selected [12,33,34]. This design was named as U-Shape design and enables a semi-free flow distribution. Fig. 3a, b and c present the selected U-Shape design and the working concept explanation.

To face all the geometrical specifications defined on the design of the prototype, an additive manufacturing (AM) fabrication process based on fused deposition modelling (FDM) was selected. This is a rapid prototyping process that enables the development of physical components based on 3D Computer-aided designs (CAD). Apart from the geometrical constrains of the prototype, system sealing, material compatibility and auxiliary system sizing were analysed. To avoid leakages, specific hydraulic gaskets were fitted creating an enclosure around the cooling channel. This gasket was defined in direct contact with the prototype enclosure, the battery cell and the proposed dielectric fluid. To ensure

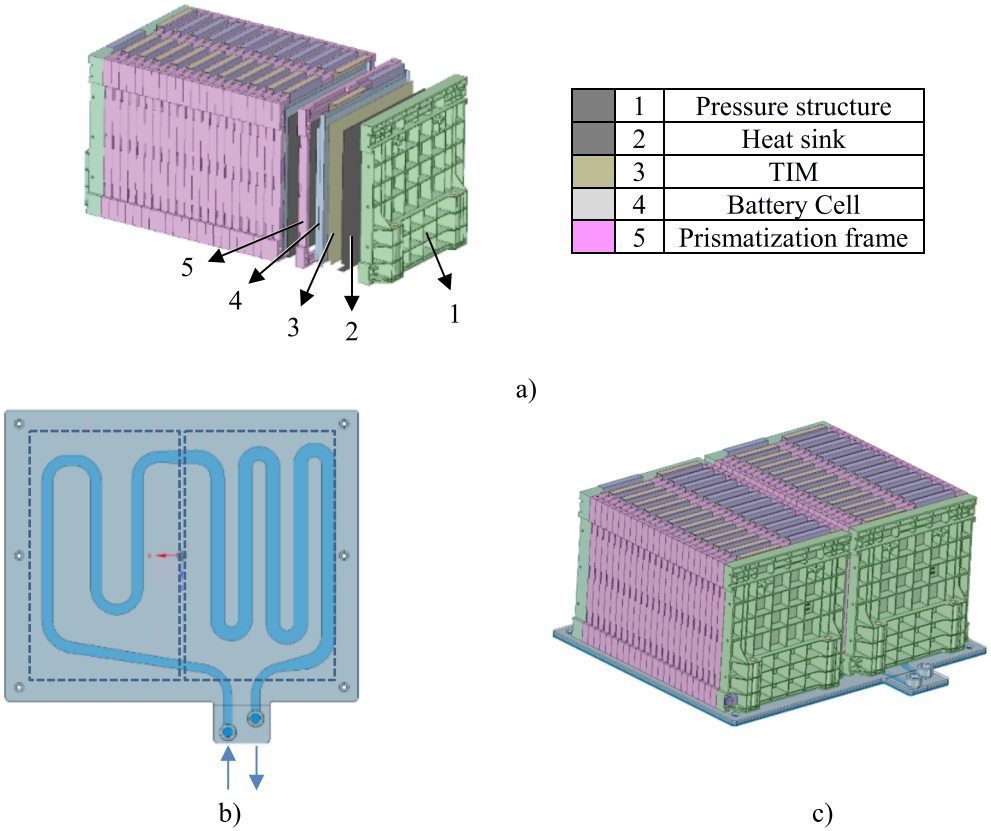

Fig. 2. Indirect Liquid Cooling (a) cell to module level scale up defining a framed linear pattern, (b) the reference cold plate hydraulic design and (c) the sub-system level assembly.

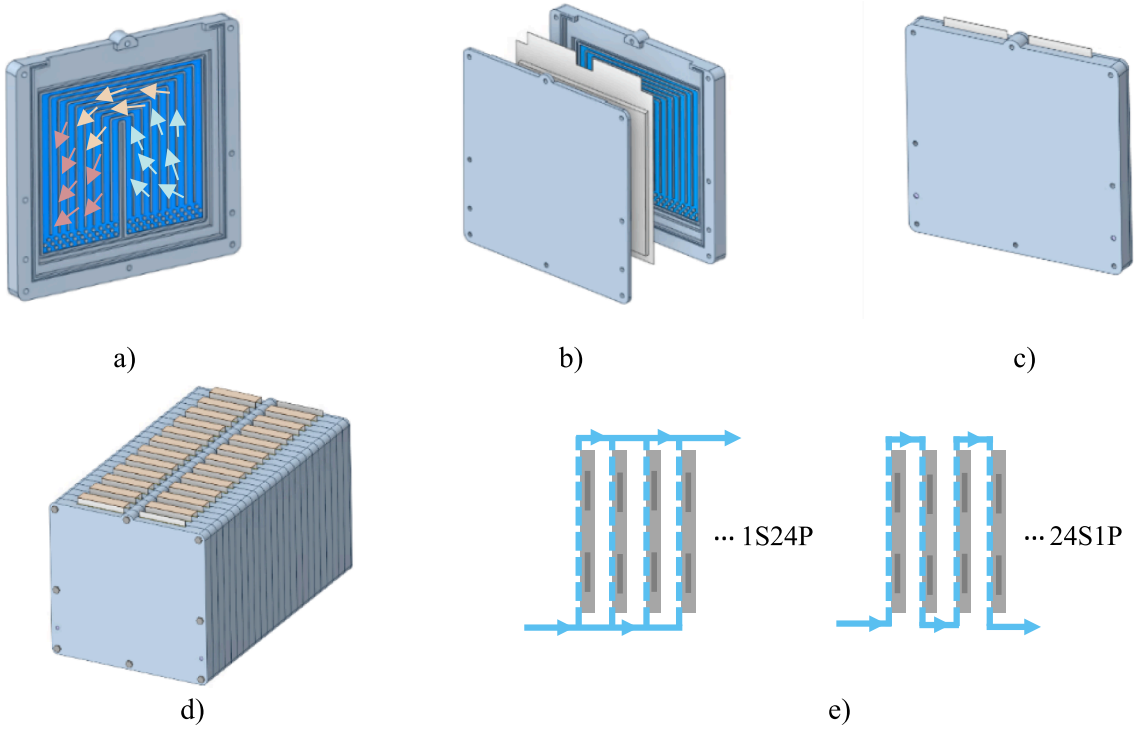

Fig. 3. Proposed prototype (a) flow pattern, (b) cell level principal components, (c) cell level assembly, (d) module level scale up and (e) the hydraulic configuration at full parallelization and full serialization.

material compatibility, all the components were selected according to the defined working conditions. Finally, to analyse the feasibility of the auxiliary system, a preliminary testing process was accomplished at different working conditions to ensure the capability of the auxiliary system to face the characteristics of the selected dielectric fluid and the applied operating conditions.

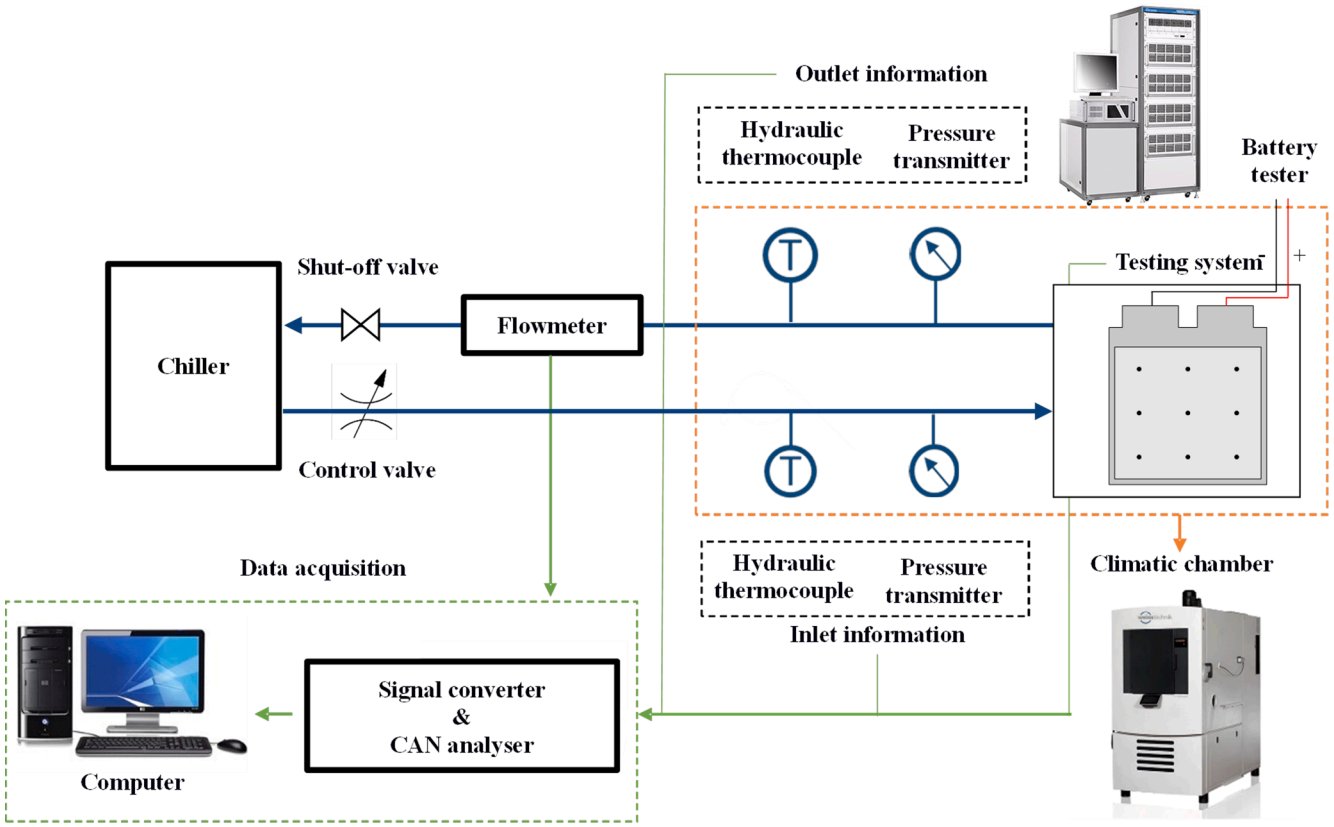

Fig. 4. Schematic overview of the experimental setup.

As it is presented in Fig. 3d, this cell level prototype was designed to enable a module level scale up developing linear patterns with isolated cell level systems. Additionally, as it is presented in Fig. 3e, the assembly of the battery module enables different hydraulic configurations (xPyS) to connect the hydraulic piping of the cell level prototypes in different ways. For the same module level flow rate, more hydraulic parallel systems reduce the flow rate per cell decreasing the heat absorption capacity of the strategy. However, at the same time, this configuration decreases the pressure drop impact and improves the thermal homogeneity of the battery system. Thus, the number of hydraulic parallelizations and serializations has to be defined on the basis of the system requirements to ensure the minimum flow rate required per cell.

3. Experimental characterization

To analyse the performance of the direct liquid cooling prototype and compare it with that of the reference module based on indirect liquid cooling, the same testing setup was defined for both strategies. Fig. 4 presents the overall schematic overview of the testing setup defined for both strategies.

To develop the testing process, separate test benches were designed for each cooling strategy. The equipment used in each case is presented in Table 2. For the ILC strategy, the main actuation components were: a Votsch VTS 4034-5 climatic chamber, to define the thermal boundary conditions of the test and to ensure the safety of the testing process; a Basytec HPS testing system, to implement the testing profiles with a temperature cut-off controller for safety; and a Lauda 5000, to control the fluid temperature and flow rate. On the other hand, on the test bench defined to analyse the proposed direct liquid cooling strategy the main actuation components were: a Weisstechnik TempEvent climatic chamber, a Chroma 17011 battery testing system, and a Lauda RE 107 thermal bath.

To analyse the information of the experimental tests, the same data acquisition components were implemented in both cases: K-type thermocouples, to measure cell temperature; a pressure transmitter (STW), to measure the pressure drop of the system; a flowmeter (Bronkhorst Mini Cori-flow), to analyse the flow rate of the fluid; an Ipetronik signal converter modules, to condition the signals of the sensors; a DC power supply; and finally a computer with a controller area network (CAN) communication protocol for data acquisition. Considering the importance of the thermal analysis of the system, the relative accuracy of the thermocouples used in the testing process was experimentally estimated by ±0.1 °C using the Weisstechnik TempEvent climatic chamber. To analyse the uncertainty of the measured parameters, a combined uncertainty analysis was developed in the appendix (Table A1).

To analyse appropriately the temperature distribution of the battery cells, different thermocouples were positioned on the surface of the battery cells. For the ILC strategy, seven thermocouples were positioned in the first cell of the first module of the sub-system in the positions represented in Fig. 5a. For the DLC proposed strategy, nine thermocouples were implemented on the non-cooled cell surface area as shown in Fig. 5b.

The fluid used in the indirect liquid cooling strategy is a commercial water glycol refrigerant (50/50 %v), whereas a dielectric fluid based on mineral oil was selected for the direct liquid cooling strategy analysed in this work. The properties of the two fluids for 25 °C are depicted in Table 3.

To analyse how each strategy manages the thermal behaviour of the battery system in different working conditions, two test situations were defined. On the one hand, a steadystate current pulse test, to analyse the capacity of the cooling strategy to control the battery thermal behaviour implementing a constant heat generation. On the other hand, a transient thermal state, a thermal scenario defined to mirror a real working condition of the battery system implementing 1.6C semi-fast charging profiles. The conditions were defined using as a reference a specific driving profile of an electric bus. Fig. 6 presents the current and voltage profiles of the steady (Fig. 6a) and transient (Fig. 6b) state scenarios, respectively. The first section of each profile corresponds to an initialization process to adequate the electrical and thermal characteristics of the battery cell. With this initial process, the same initialization is guaranteed for different tests.

Furthermore, a deep semi-fast charge of 2C from 0% to 100% SOC and a deep semi-fast discharge of 3C from 100% to 0% SOC were implemented to analyse the capacity of the DLC cooling strategy to face high cooling demand situations.

4. Experimental results and discussion

The experimental analysis is divided into three main sections. First, based on the pumping power consumption of the indirect liquid cooling-based sub-system, the reference flow rate defined for the proposed prototype tests is calculated. Then, the performance of the proposed direct liquid cooling strategy is analysed by defining capacitance, steady-state, and deep semi-fast charge and discharge tests. Finally, a comparison with the indirect liquid cooling strategy is developed to highlight the advantages of the proposed direct liquid cooling strategy.

4.1. Pressure drop and pumping power analysis

The reference flow rate defined for the proposed prototype tests was calculated based on the pumping power consumption of the indirect liquid cooling-based sub-system. In a real working condition, the ILC battery sub-system works with a flow rate of 2 L/min. The pumping power loss related to the cold plate is calculated by multiplying the flow rate and the pressure drop of the component. Therefore, the cold plate was experimentally tested to analyse the pressure drop variation of the component at different flow rates. The results of the study are depicted in Fig. 7a. From this analysis, pumping power consumption of 0.81 W was measured for the reference flow rate of 2 L/min.

The cold plate was used to manage the thermal behaviour of a sub-system composed of 2 modules (48 battery cells). Therefore, to be able to compare it with this strategy, a scale up to a sub-system level had to be

Table 2
Indirect liquid cooling test bench and direct liquid cooling test bench reference equipment technical data.

Equipment	Model	Parameter	Specification	Accuracy
Climatic chamber	Votsch VTS 4034–5	Temperature range	−42/180 °C	±0.5 °C
	Weisstechnik TempEvent		−42/180 °C	±0.5 °C
Battery tester	Basytec HPS	Power range	±240A//0–6 V	±0.02%//±0.05 %
	Chroma 17,011		±100A//1.5–6 V	±(0.02% RD + 0.02% of FS)//±0.05%
Chiller	Lauda 5000	Maximum flow rate and temperature range	37 L/min//−20/40 °C	±0.05 °C
	Lauda RE 107		17 L/min//−35/120 °C	±0.05 °C
Signal converter	Ipetronik M-thermo 16	Temperature range	−60/1370 °C	±0.025%
	M-sense 8	Current and voltage range	0/20 mA//0–10 V	±0.5%//±0.15%
Flowmeter	Bronkhorst Mini Cori-flow	Flow rate range	0–6.5 L/min	±0.2% RD
Pressure transmitter	STW C-02	Pressure range	0–1 bar	±0.3% FS
Thermo-couple	K-type	Temperature range	−30/1100 °C	±0.1 °C (estimated)

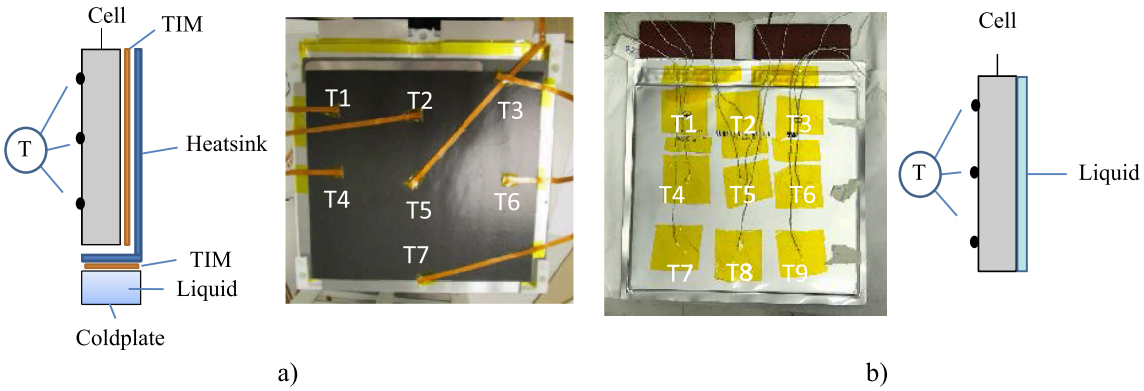

Fig. 5. Schematic representation and picture of the thermocouple disposition of the (a) indirect liquid cooling and (b) direct liquid cooling strategies.

Table 3
Properties of water glycol 50/50 %v and the dielectric fluid, for 25 °C.

Property	Water glycol 50/50 %v	Dielectric fluid
Resistivity (MΩm)	–	$>5 \cdot 10^6$
Kinematic viscosity (mm^2/s)	2.58	4.3
Specific heat capacity (J/kgK)	3473	2130
Thermal conductivity (W/mK)	0.37	0.135
Density (kg/m^3)	1062	774

performed first with the proposed direct liquid cooling strategy. To analyse the equivalent power consumption of the cell level prototype, the previously calculated value of 0.81 W was divided by the number of total cells per sub-system (48 battery cells) yielding 0.016 W per cell. To determine the working point at which the proposed direct liquid cooling strategy equates to the defined power consumption, the prototype was experimentally tested at different flow rates to analyse the pressure drop variation. From the measured characteristic curve shown in Fig. 7b, the reference flow rate with which the prototype equals the pumping power requirement per cell was determined as 0.43 L/min. These tests were performed at 25 °C for both cases.

To define a comparable sub-system level working condition, a theoretical module level scale up was defined to match the system pumping power consumption of both strategies. This theoretical module of 24 cells was divided into six sub-modules of four cells. For each sub-module an internal parallelisation of 1S4P was defined. Therefore, the defined module was based on a 6S4P hydraulic configuration.

The proposed flow rate and configuration equals the power consumption of the indirect liquid cooling strategy and reduces by 14% (from 2 L/min to 1.72 L/min) the flow rate needed for the sub-system. Hence it can be concluded that the implementation of a direct liquid cooling module would not result in an increase in the pumping power consumption of the system.

4.2. DLC prototype thermal analysis

In the second part of the analysis the thermal performance of the prototype is characterised. First, a capacitance study was developed without any heat generation to analyse the influence of the environmental conditions. Then, steady-state tests were implemented to analyse the capacity of the proposed prototype to meet the working conditions demanded by the system when the battery cell is generating heat. In these tests, a constant heat generation was implemented by 1C and 2C current pulse profiles. Taking advantage of this situation, the influence of the flow rate and the fluid temperature on the thermal response of the battery cell was analysed. Finally, deep semi-fast charge and discharge tests were implemented to analyse how the proposed strategy responds to high cooling demands.

4.2.1. System capacitance tests

Defining 25 °C as the reference temperature value for the refrigeration fluid, the environment temperature effect was analysed at 30 °C, 35 °C, and 40 °C, to determine the interaction between the prototype and the environment. The starting point of all tests was defined at 25 °C and

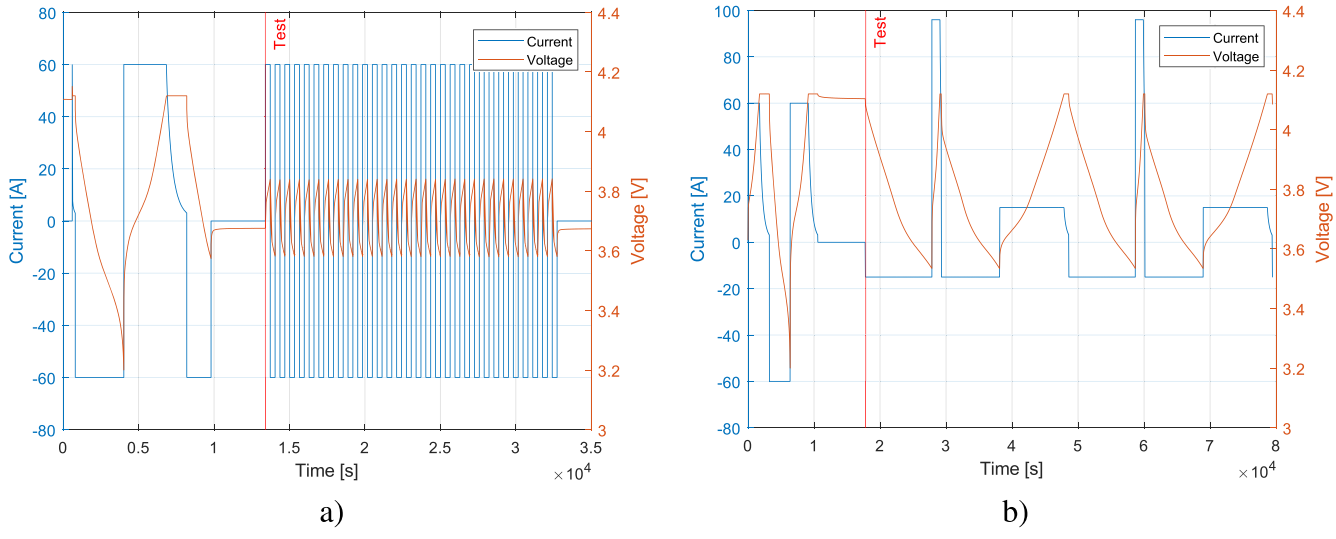

Fig. 6. Current and voltage profiles of (a) steady-state and (b) transient state tests.

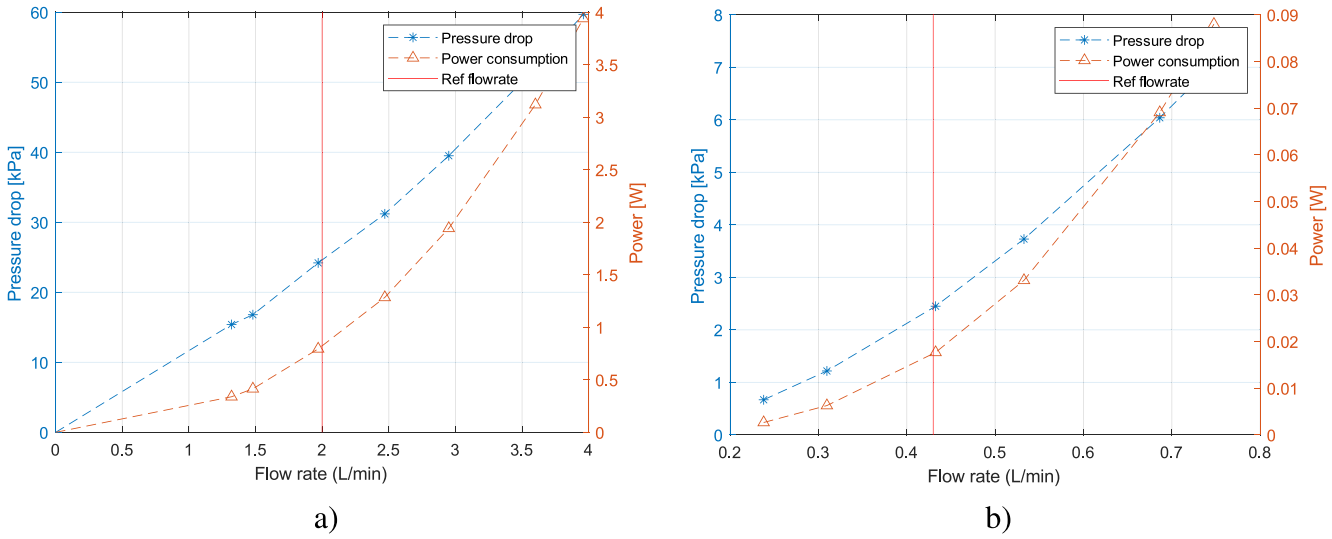

Fig. 7. Experimental pressure drop variation for (a) ILC strategy, and (b) the proposed DLC strategy at different flow rate values and the reference power consumption of each strategy.

the of the climatic chamber was consecutively increased to the defined values. Constant flow rate was defined at 0.43 L/min for all tests.Fig. 8 presents the transitory cell and tab temperature results of each test.

As Fig. 8 shows, although the inlet fluid temperature is defined at 25 °C, the temperature of the battery cell increases with the boundary temperature increase. This means that there was an external influence that affected the cell temperature. Analysing the cell tab temperature, it can be observed that the environment has a greater influence on these components. The reason for this is that tabs are located outside the prototype enclosure to facilitate the connection of the power cables to the cell. They are directly welded to the internal layers of the battery cell, an arrangement that facilitates heat transfer between the tabs and the cell body. Therefore, the influence of the environment on the tabs affects the cell temperature. However, as presented in Table 4, the cooling effect of the strategy stabilised cell temperature much lower than tab temperature, and this difference increased in each test. This result demonstrates that the cooling strategy has a greater influence on the battery cell than the environment.

To visualise the interaction between the environment and the battery cell, in Fig. 9 the stationary temperature distribution of the battery cell is presented. As can be observed, the most influenced area by the external temperature is the area of the tabs, results in line with the developed analysis. In accordance with the results of Table 4, the larger the difference between the fluid temperature and the ambient temperature, the greater the increase in the temperature heterogeneity of the cell.

To quantify the influence of the environment on the cooling strategy, the equivalent external thermal resistance was evaluated. Assuming that

Table 4
Battery cell and tab stationary temperature results at environment temperatures of a) 30 °C, b) 35 °C, and c) 40 °C.

T_{amb} (°C)	$T_{c,mean}$ (°C)	ΔT_c (°C)	T_{t_mean} (°C)	$\Delta T_{c,t}$ (°C)
30	27.1	0.2	28.4	1.2
35	29.3	0.5	31.7	2.4
40	31.5	0.7	35.2	3.7

all the heat absorbed by the fluid is rejected by the environment, the heat dissipated by the fluid was calculated by equation $Q{=}\dot{m}c_p\Delta T$. Where $\dot{m}$ was the mass flow rate of the refrigeration fluid, ΔT the difference between average fluid inlet and outlet temperatures, and c_p the specific heat capacity value of the dielectric fluid. The numerical results of the heat absorbed by the fluid are set out in Table 5, which shows that the heat absorbed by the fluid increases proportionally with the ambient temperature increase.

The equivalent external thermal resistance between the environment and the fluid was calculated by equation $R = \Delta T/Q$. Where ΔT was the difference between ambient temperature and fluid mean temperature, and Q the heat transferred by the environment. The experimental and numerical values of the calculation process are depicted in Table 5. As presented, although the heat absorbed by the fluid increases in proportion to the increase of the boundary temperature, the resistance value remains stable showing that it is a characteristic of the system itself. This result evidence the robustness of the developed analysis and

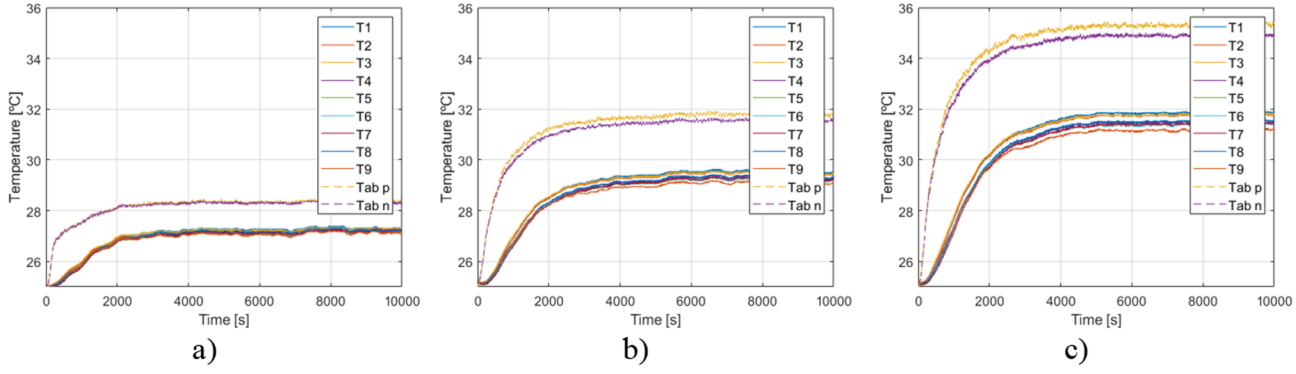

Fig. 8. Battery cell and tab transitory temperature results at environmental temperatures of (a) 30 °C, (b) 35 °C, and (c) 40 °C.

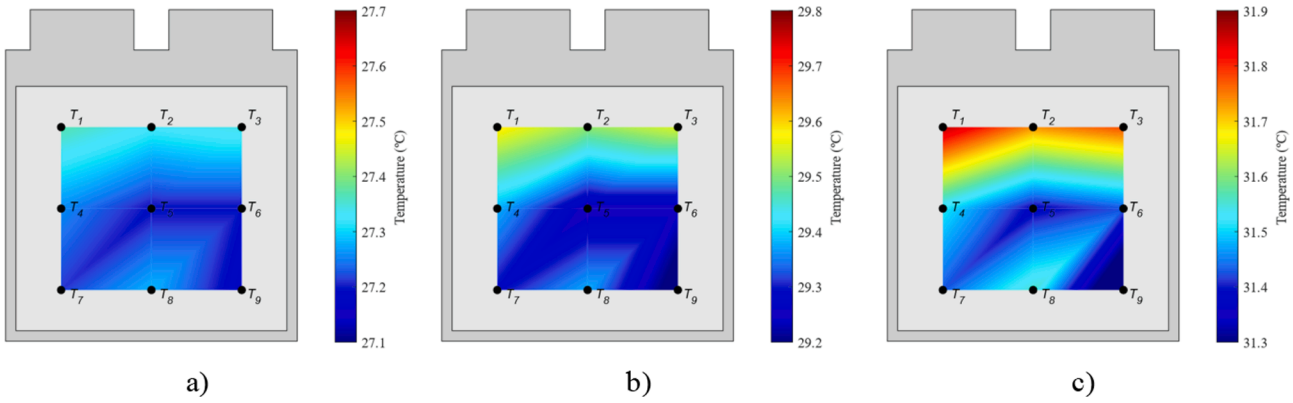

Fig. 9. Thermal stabilization map of the battery cell using postprocessed thermocouple temperature information at environment temperatures of (a) 30 °C, (b) 35 °C, and (c) 40 °C.

Table 5
Equivalent external thermal resistance calculation between the environment and the cooling strategy at ambient temperatures of 30 °C, 35 °C, and 40 °C.

Ambient temperature (°C)	30	35	40
Flow rate (L/min)	0.43	0.43	0.44
Fluid ΔT (°C)	1.0	2.1	3.1
Fluid absorbed heat (W)	12.22	25.02	38.02
Fluid mean temperature (°C)	25.8	26.5	27.2
Equivalent resistance (K/W)	0.34	0.34	0.33

allows to evaluate the contribution of the environment in the following tests where the battery cell is actively working generating heat.

4.2.2. *Steady-state tests*

Steady-state pulse tests were implemented to analyse the capacity of the proposed direct liquid cooling prototype to respond to the working conditions demanded by the system when the battery cell is generating heat. To control the influence of the variables of the system, constant heat generation tests were defined by specifying 1C and 2C charge–discharge pulse tests, as shown in Fig. 6. This test works between 50 % and 60 % of the SOC level of the battery cell to ensure a similar heat generation in charge and discharge processes. This constant heat generation enables the analysis of the stationary thermal response of the battery cell. Under these controlled conditions, the influence of the working variables on the performance of the proposed strategy can be properly analysed. In this analysis, dielectric fluid inlet temperature and flow rate were defined as the variables of interest. A minimum set of three tests were defined for each variable to observe how the system controls the thermal behaviour of the battery cell.

- Effect of dielectric fluid inlet temperature

To analyse how the fluid temperature can impact the thermal behaviour of the battery cell, ambient temperature was set at 25 °C and the fluid flow rate variable was defined as 0.43 L/min, the reference value that was calculated to equal the pumping power consumption of the indirect and direct liquid cooling strategies. To have a comparable starting point for the comparison, all tests started from an initialization temperature of 25 °C, to have a comparable starting point for the comparison. Testing fluid temperatures at 10 °C, 25 °C, and 40 °C, were defined to analyse the capacity of the fluid to impact the heating, cooling, and thermal maintenance of the system. The battery cell transitory temperature results of each test are presented in Fig. 10, and the temperature, pressure, and power consumption results of the thermal stabilization section are set out in Table 6.

Fig. 10 shows that the DLC strategy can decrease the temperature of the battery system even when the cell generates heat during operation and the ambient conditions are adverse (Fig. 10c). The temperature heterogeneity is another variable to analyse. The highest battery cell temperature difference of 1.5 °C can be found in the test where the fluid inlet temperature was defined at 10 °C (Fig. 10a). This result is due to the effect of the environment on the cell. Considering that the environment has greater influence on the upper part of the battery cell and

Table 6
Stationary temperature, pressure drop, and power consumption mean values of tests at 10 °C, 25 °C, and 40 °C dielectric fluid inlet temperatures.

T_f (°C)	$\dot{V}_{mean}$ (L/min)	$T_{c,mean}$ (°C)	$T_{c,max}$ (°C)	ΔT_c (°C)	ΔT_f (°C)	ΔP (kPa)	P_h (mW)
10	0.44	19.0	19.8	1.5	4.3	3.46	25.8
25	0.44	26.5	26.8	0.5	0.3	2.74	20.3
40	0.44	34.1	34.5	0.5	−3.8	2.10	15.9

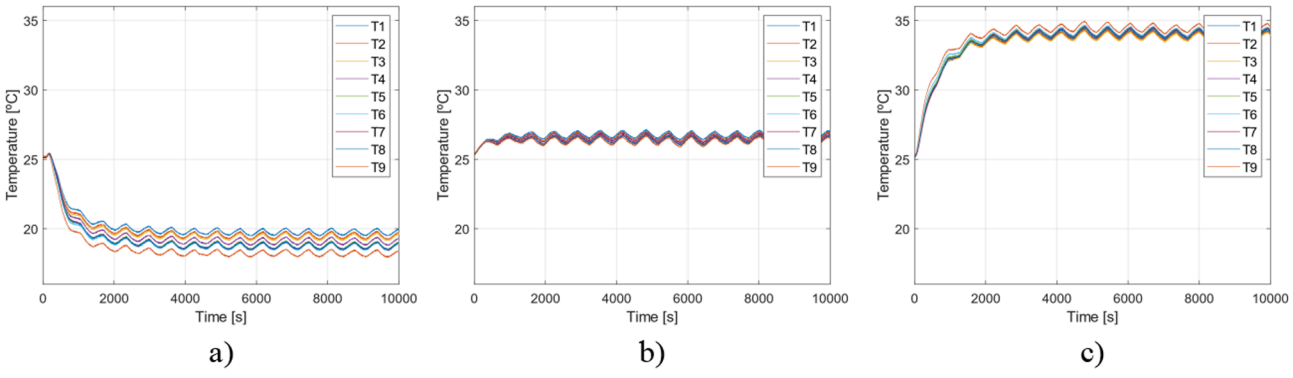

Fig. 10. Battery cell temperature distribution at (a) 10 °C, (b) 25 °C, and (c) 40 °C dielectric fluid inlet temperatures, with 25 °C ambient temperature.

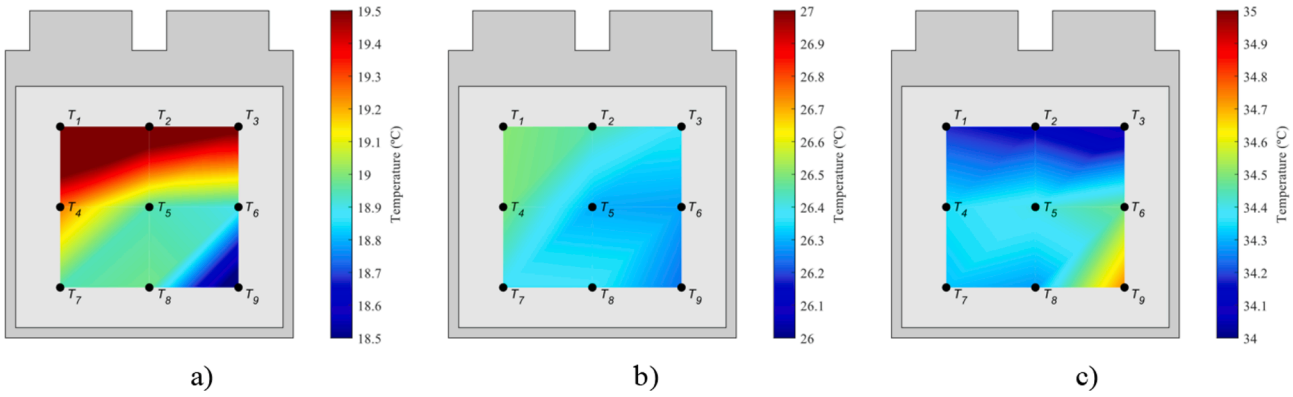

Fig. 11. Thermal stabilization map of the battery cell using postprocesses thermocouple temperature information at fluid inlet temperature of (a) 10 °C, (b) 25 °C, and (c) 40 °C.

the effect of the tab heat generation is more pronounced in this area, it can be concluded that when the ambient temperature is above the temperature of the fluid, the thermal gradient of the system increases.

The influence of the fluid temperature on the pressure drop of the system is another result that is worth highlighting. The main fluid variables that can affect the pressure drop of the system are velocity and viscosity [35]. All tests were conducted using the same flow rate, thus, temperature change was directly affecting the properties of the fluid. At low temperatures, the molecular cohesive force of the fluid increases, causing the viscosity to increase, and this variable directly influences the pressure drop of the system. As the temperature of the fluid was increased from 10 °C to 25 °C, to 40 °C, the pressure drop decreased from 3.46 kPa to 2.74 kPa, to 2.10 kPa, respectively. The pumping power of the system was calculated, and the influence of the fluid temperature was observed. Compared to the test where the fluid reference temperature was set to 10 °C, the power consumption was reduced by 20.9 % and 38.7 % in the tests with a fluid temperature of 25 °C and 40 °C, respectively.

Using the flow rate and fluid temperature results, the heat absorbed or rejected by the fluid can be calculated. A heat absorption of 52.4 W was calculated from the test in which the inlet fluid temperature was defined at 10 °C. Using the information from Fig. 1b, it was calculated that the battery cell generates 5.27 W at 1C tests working at values between 50% and 60% of SOC. Therefore, 47 W of heat was transferred from the environment to the fluid. In the case of the test where the fluid inlet temperature was 40 °C, the same heat quantity was transferred from the fluid to the environment. Therefore, it can be determined by equation $R = \Delta T/Q$ that the interaction between the environment and the cooling strategy is 0.3 K/W. Result in accordance with the external thermal resistance calculated with the capacitance tests.

To analyse how the cell is influenced by the environment, in Fig. 11 the stationary thermal behaviour of the cell is presented for each case. Results show that the greatest interaction with the environment is seen in the area of the tabs, a result that agrees with that analysed in the capacitance tests.

- Effect of dielectric fluid flow rate

To analyse the influence of the fluid flow rate on the temperature distribution of the cell and on the power consumption of the system, tests at 0.21 L/min, 0.32 L/min, 0.43 L/min, 0.53 L/min, and 0.64 L/min were carried out. To have a higher heat generation rate and thus, properly observe the difference of the thermal results, 2C charge–discharge pulse tests were defined in these tests. Ambient and fluid inlet temperatures were defined at 25 °C in all tests. Fig. 12 presents the transitory results until the stabilization point of the most representative tests. Stationary mean values of each test are set out in Table 7.

As it is depicted in Fig. 12, with the increment of the fluid flow rate the temperature of the battery cell decreases, and the thermal homogeneity increases. Moreover, the time needed for the cell to thermally stabilise is reduced. However, as is shown in Table 7, the impact on the system pressure drop is more relevant than the impact on the thermal behaviour.

As expected, the pressure drop of the system was influenced by the change of the flow rate. This phenomenon is based on the equation of Darcy–Weisbach [35], where it is presented that the velocity of the fluid has a squared influence on the pressure drop of the system. This influence affects the pumping power consumption of the system as shown in Table 7. Power consumption was decreased from 58.9 mW to 2.4 mW, with the decrease of the flow rate from 0.64 L/min to 0.21 L/min, respectively. Although the pumping power of the system was dramatically affected by the variation of the flow rate, the temperature of the

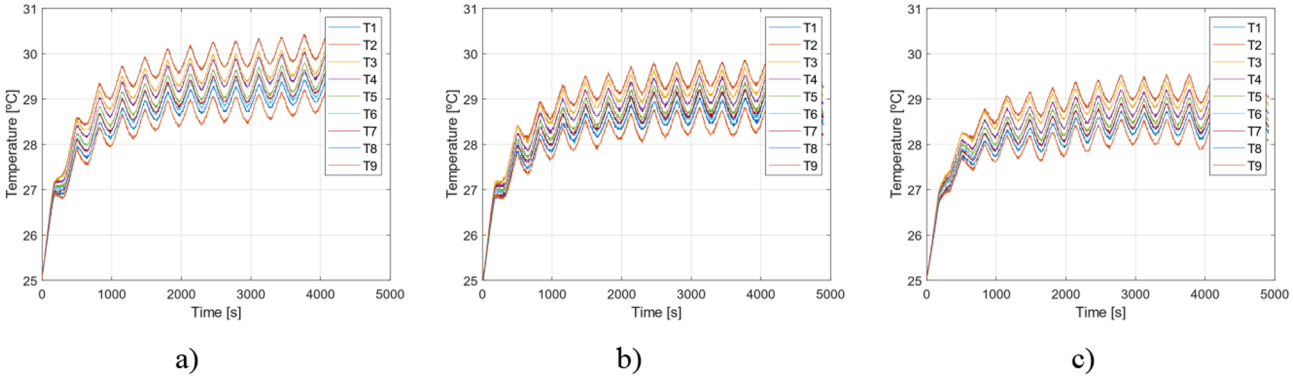

Fig. 12. Battery cell temperature distribution at (a) 0.21 L/min, (b) 0.43 L/min, and (c) 0.64 L/min of dielectric fluid flow rate.

Table 7
Stationary temperature, pressure drop, and power consumption mean values of tests at 0.21 L/min, 0.32 L/min, 0.43 L/min, 0.53 L/min, and 0.64 L/min.

V_{mean} (L/min)	$T_{c,mean}$ (°C)	$T_{c,max}$ (°C)	ΔT_c (°C)	ΔT_f (°C)	ΔP (kPa)	P_h (mW)
0.21	29.6	30.1	1.2	1.6	0. 74	2.4
0.32	29.4	29.8	1.2	1.1	1.61	8.7
0.43	29.2	29.5	1.1	0.9	2.78	20.2
0.53	29.0	29.4	1.0	0.7	4.18	38
0.64	29.0	29.2	1.0	0.6	5.54	58.9

battery cell remains stable near 30 °C. This means that the proposed direct liquid cooling strategy can keep the battery cell temperature within the optimum operating temperature range even if the flow rate is considerably reduced. Result that directly affects the auxiliary system sizing and the pumping power consumption. As it is presented in Fig. 13, with the increase of the flow rate, even if the power consumption increases significantly, the impact on the temperature heterogeneity of the battery cell is minimum.

The heat absorbed by the fluid was calculated using flow rate and fluid temperature results of Table 7. In a range between 9.4 W and 10.6 W, the mean heat absorbed by the fluid in all tests was 10.1 W. Using the information of Fig. 1a, it was calculated that the battery cell generates

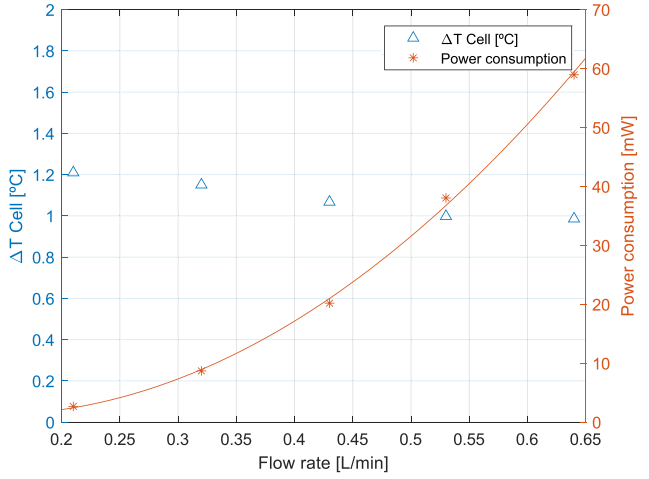

Fig. 13. Power consumption and battery cell thermal heterogeneity values.

15.25 W at 2C tests working at values between 50% and 60% of SOC. Therefore, the results presents that the third part of the heat generated by the cell is rejected to the environment. This effect is since at high charge and discharge ranges the tabs becomes in hot spots. The high current density passing through the tabs causes the heat generation of these components to increase due to the joule effect. Therefore, considering that tabs are in direct contact with the environment, it is reasonable that one part of the heat generated on the cell is transferred in this way.

4.2.3. *Deep semi-fast charge and discharge analysis*

To analyse how the strategy proposed can face high cooling demands, deep semi-fast charge (0–100% SOC) and discharge (100–0% SOC) tests were performed. To this end, 2C semi-fast charge and 3C semi-fast discharge tests were defined to analyse the effect of high cell heat generation scenarios. In both tests, flow rate, fluid inlet temperature and environment temperature were fixed at 0.43 L/min, 25 °C, and 25 °C, respectively. Battery cell temperature results of the constant current (CC) section of each test are presented in Fig. 14 with the corresponding cell voltage values. Temperature profiles of both tests have the same shape as the heat generation profile depicted in Fig. 1b.

Semi-fast charge and discharge current profiles implemented on these tests were defined to analyse how the proposed strategy manages the thermal behaviour of the selected battery cell on the maximum working requirements. This high heat generation scenarios happen when the charging time of the electric vehicle reduces, increasing proportionally the current profile implemented on the process. At those levels, as it is presented in Fig. 14, the heat generated by the battery cell increases making it difficult to keep cell temperature in the optimal operating range. To analyse how the cell was influenced, thermal values of the maximum temperature working section of the transitory testing results are depicted on Table 8. The proposed strategy maintains the temperature of the battery cell below 40 °C in both cases. Managing the thermal behaviour of the system within the optimal operating range.

Table 8
Thermal values of 2C semi-fast charge and 3C semi-fast discharge tests selected from the maximum temperature working section of the transitory testing results.

Test	V_{mean} (L/min)	$T_{c,mean}$ (°C)	$T_{c,max}$ (°C)	ΔT_c (°C)	ΔT_f (°C)	Q_f (W)
CC2C	0.45	31.18	31.38	0.96	1.81	22.9
DC 3C	0.45	37.69	38.00	1.28	3.27	41.2

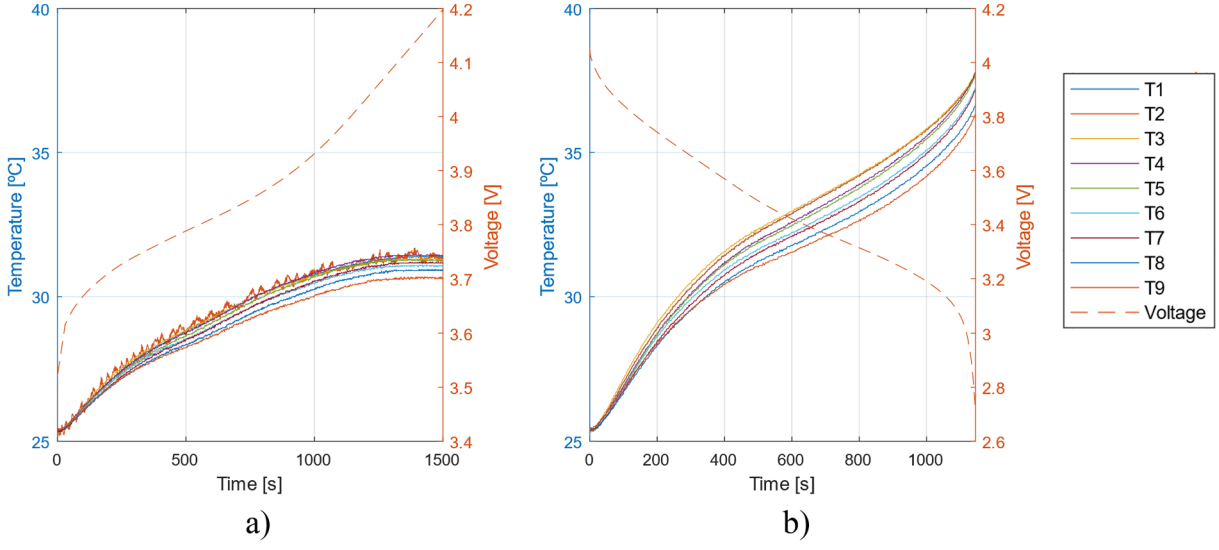

Fig. 14. Battery cell temperatures for (a) 2C semi-fast charge and (b) 3C semi-fast discharge tests.

Analysing the calorimeter tests developed in Fig. 1, it was calculated that 29.6 W and 49.8 W were generated by the cell in the maximum heat generation point (maximum temperature points of the tests) at 2C deep charge and 3C deep discharge tests, respectively. Which means that the fluid has absorbed the 77 % and 82 % of the heat released by the cell, respectively. These results show that the higher the heat generation of the cell, the greater the effectiveness of the proposed strategy is.

4.3. Comparison between indirect and direct liquid cooling strategies

To highlight the advantages of the proposed direct liquid cooling strategy, first, a comparison with the indirect liquid cooling strategy was developed defining steady-state 1C pulse tests. To generate comparable results, the last sub-module of the proposed direct liquid cooling subsystem (two hydraulically serialized DLC modules) was selected. According to the hydraulic serialization defined in section 4.1, this is the last sub-module of the hydraulic serialization composed of twelve submodules (six sub-modules per module) with the worst working casuistry. Therefore, to characterise the working conditions, some adequations were proposed.

First, the inlet temperature of the fluid was modified to mirror the inlet temperature of the proposed sub-module. This input was calculated analysing how much heat generates the selected battery cell at 1C charge–discharge process, information presented in Fig. 1. To mirror the SOC level of the steady-state tests, values between 50% and 60% of SOC were selected to calculate the mean heat generation value of 5.27 W. This heat generation was used to calculate the fluid temperature difference between the inlet and the outlet of a cell level prototype by the equation $\Delta T = Q/\dot{m}c_p$. Where Q was heat generated by the cell, $\dot{m}$ the mass flow rate of the refrigeration fluid, and c_p the specific heat capacity value of the dielectric fluid. In this way, a fluid temperature difference of 0.44 °C was calculated. Implementing this temperature difference on the proposed sub-system for the direct liquid cooling strategy, an inlet temperature of 29.8 °C was calculated for the last sub-module of the subsystem. This inlet temperature was defined on the comparison tests for the direct liquid cooling strategy. For the indirect liquid cooling strategy, an inlet temperature of 25 °C was maintained.

Then, to isolate the influence of the environment from the comparison, an ambient temperature higher than the cell temperature of the last cell of the sub-system was defined to prevent heat transfer from the battery cell to the environment. This temperature was calculated considering the heat generated by the battery cell and the fluid inlet temperature for the last sub-module of the sub-system (29.8 °C). With this approach, a mean temperature value of 31.3 °C was calculated for the last cells of the proposed sub-system. To ensure that the environment temperature was set above the cell temperature, a value of 33 °C was defined for the ambient temperature on the direct liquid cooling test.

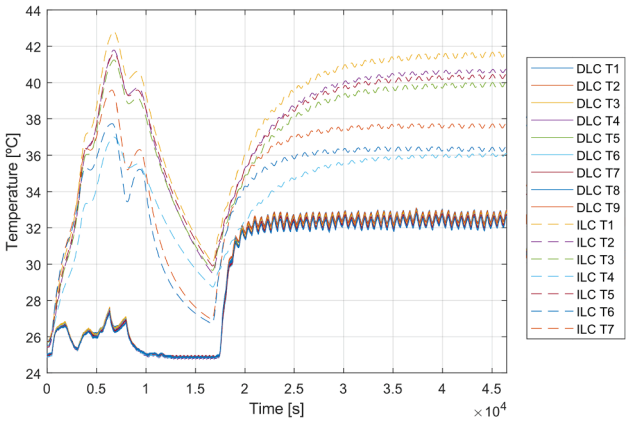

Fig. 15. Transitory temperature values for Indirect Liquid Cooling and Direct Liquid cooling Pulse tests.

Table 9
Thermal stabilization temperature values for Indirect Liquid Cooling and Direct Liquid cooling Pulse tests.

Tets	$T_{f,in}$ (°C)	T_{amb} (°C)	$T_{c,mean}$ (°C)	$T_{c,max}$ (°C)	ΔT_c (°C)
ILC	25	25	38.9	41.7	5.7
DLC	30.51	33	32.4	32.6	0.4

This value was experimentally validated to ensure that the environment had no capacity to absorb heat from the cell. On the other hand, the indirect liquid cooling strategy was tested at an ambient temperature of 25 °C. Fig. 15 presents the transitory temperature results of each strategy, and the results of the thermal stabilization section are set out in Table 9.

Even the working conditions of the testing process were defined to mirror the worst case of study, results of Fig. 15 present the high capacity of the proposed strategy to control the temperature of the battery cell. With a thermal heterogeneity of 0.4 °C, cell mean temperature is maintained at 32.4 °C with an input fluid mean temperature of 30.5 °C. On the other hand, mean temperature and the thermal heterogeneity of the battery cell tested with the indirect liquid cooling strategy were stabilized at 38.9 °C and 5.7 °C, respectively. Difference that highlights the higher thermal management capacity of the proposed direct liquid cooling strategy. To analyse the influence of the environment on the proposed strategy, the heat absorbed by the fluid was calculated. With a fluid temperature difference of 0.6 °C between the inlet and the outlet of the direct liquid cooling prototype, it was calculated that the fluid has absorbed 7.4 W of heat, 1.7 W more than the heat generated by the cell. This heat was transferred from the environment worsen the casuistry defined for testing and confirms that the environment did not has a positive influence on the results of the proposed prototype.

Thermal resistance values of 0.22 K/W and 2.53 K/W were estimated between the fluid and the battery cell with the comparative results for the direct and indirect liquid cooling strategies, respectively. A difference between results of one order of magnitude. This approach highlights the improvement of the direct liquid cooling strategy over the indirect one.

Finally, to analyse the working efficiency of the strategies, Table 10 presents the pumping power consumption referenced on each of the tests showed in Fig. 15. The power consumption in a sub-system level is defined at 0.81 W and 0.9 W for the indirect and direct liquid cooling strategies respectively. Result that confirms the feasibility to implement direct liquid cooling strategy without modifying the power consumption ranges of the system. It is concluded therefore that the proposed strategy in this work has the potential to improve the efficiency of the overall system, implementing a more accurate thermal management control without changing the power consumption ranges of the system.

To analyse how the proposed strategy controls the temperature of the battery cell at real working conditions, transient tests were implemented. These tests mirror the driving profile of an electric vehicle implementing the equivalent current profile of each working casuistry. In this case, the route of an electric bus was characterized, and the equivalent current profile was calculated. As presented in Fig. 6, the characterized driving route has different C/4 charging and discharging profiles and a semi-fast charge of 1.6C, where the battery system is charged from 20% to 90% SOC in 26 min. A casuistry where the cooling strategy has to manage high heat generation profiles.

The objective of this comparison is to analyse how the performance of the cooling strategy influences the thermal response velocity of the

Table 10
Pumping power consumption of direct and indirect liquid cooling strategies.

Tets	V_{mean} (L/min)	ΔP (kPa)	$P_{h,c}$ (W)	$P_{h,ss}$ (W)
ILC	2	24.2	–	0.81
DLC	0.45	2.5	0.019	0.91

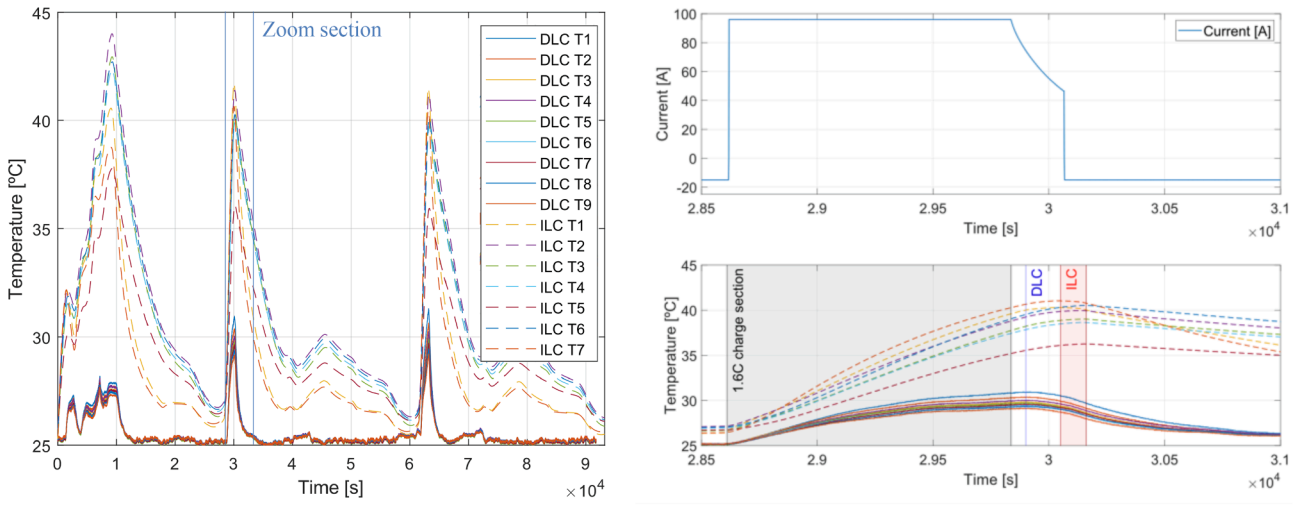

Fig. 16. Temperature transient values for indirect and direct liquid cooling strategies in (a) the whole test, and (b) current and temperature and current values of the zoomed section.

battery system and controls the maximum temperatures. For that, same boundary conditions were implemented on each test. Constant values of fluid inlet temperature and ambient temperature were defined at 25 °C. The definition of the flow rate was based on the calculations made to equal system pumping power consumptions of both strategies. 0.45 L/min and 2 L/min for direct and indirect liquid cooling strategies, respectively. The initialization temperature was defined at 25 °C. Fig. 16 presents the transitory temperature results of each test.

Fig. 16 presents the influence of the thermal management strategy on the thermal control velocity. As it is mentioned, the indirect liquid cooling strategy has a larger thermal resistance network between the battery cell and the refrigeration fluid that slows down the refrigeration effect of the strategy. Casuistry that defines the temperature control velocity of the battery cells. Considering testing results from Fig. 16a, the battery cell based on indirect liquid cooling has difficulties to face the temperature increase defined on the semi-fast charge before the second driving cycle arrives. The delay in temperature response is partially linked to the larger thermal resistance network defined on the strategy and presents the difficulties that has the heat to move from the battery cell to the cooling fluid.

Fig. 16b zooms the current and temperature values nearby the semi-fast charge section. It is noted that each strategy starts reducing cell temperature at different times after the semi-fast charge. The characteristic of contacting the battery cell directly with the cooling fluid enables the proposed strategy to start reducing all cell temperatures at the same moment, approximately 1.15 min after the current profile starts decreasing. In the case of indirect liquid cooling strategy, due to the larger thermal resistance, the cell did not respond to cooling until 3.8 to 5.75 min after the current started decreasing. Moreover, as the red band of Fig. 16b presents, this cooling profile was not reached to the cell homogeneously, influencing first the low part of the cell (3.8 min) and then the top part (5.75 min).

5. Conclusions

In this work, an innovative direct liquid cooling strategy for the thermal management of large-scale pouch type lithium-ion batteries is proposed, focusing on the cooling effect on one area of the battery cell instead of immersing the battery system in the dielectric fluid. A cell level prototype was developed with a modular design, and its performance was experimentally evaluated. To analyse the effectiveness of the proposed strategy, a comparison with the indirect liquid cooling strategy was conducted based on the pumping power consumption criterion. From the results, the following conclusions can be drawn:

- The power consumption was decreased from 58.9 mW to 2.4 mW at 2C pulse tests, when the flow rate was decreased from 0.64 L/min to 0.21 L/min, respectively. Scaling up this scenario to a sub-system level, the proposed strategy makes it possible to improve the efficiency of the auxiliary system, by reducing the flow rate and increasing the number of hydraulic parallelizations implemented in the system.
- The proposed strategy can address high heat generation situations. At 2C and 3C semi-fast charge and discharge tests, cell maximum temperatures and heterogeneity were maintained below 38 °C and 1.3 °C, respectively. These temperatures are within the optimal operating range.
- Comparing the proposed strategy at steady-state 1C pulse tests to the indirect liquid cooling strategy, the maximum temperature of the battery cell decreased from 41.68 °C to 32.58 °C, while the homogeneity dropped from 5.71 °C to 0.36 °C. More accurate temperature control at the same pumping power consumption confirms the higher performance of the proposed strategy.
- The results of the comparative test show that the thermal resistance value between the fluid and the cell of the proposed strategy was 0.22 K/W, an order of magnitude lower than that of the indirect liquid cooling strategy. Owing to this characteristic, the cell temperature was reduced instantaneously and homogeneously to the cooling setpoint after semi-fast charges with the proposed strategy.

With more accurate thermal management control and without the need to increase the power consumption of the auxiliary system, the proposed strategy improves the performance of the battery system. It can thus be concluded that the implementation of this strategy can increase the life of the battery system, reduce the size and power consumption of the auxiliary system, and facilitate BTMS strategy control implementation.

Declaration of Competing Interest

The authors declare that they have no known competing financial interests or personal relationships that could have appeared to influence the work reported in this paper.

Acknowledgments

This research did not receive any specific grant from funding agencies in the public, commercial, or not-for-profit sectors.

Appendix A. . Uncertainty analysis

The uncertainty analysis was conducted considering all the components that affect the measured signal. It was therefore calculated for each variable of study the combined expanded uncertainty in Table A1. This combined uncertainty, apart from the accuracy of the measurement's instruments, considers the standard deviation and the resolution of the signal converters for each of the variables of the study.

Table A1
Combined uncertainty analysis.

Variable	Range	Instrument accuracy	Combined Expanded Uncertainty
Ambient temperature (climatic chamber)	[10–45] °C	± 0.5 °C	± 0.5 °C
Temperature (thermocouple)	[10–45] °C	± 0.1 °C (estimated)	± 0.101 °C
Pressure	[0–60] kPa	±0.3% FS	± 0.2 kPa
Volumetric flow rate	[0–2.15] L/min	± 0.2% RD	± 0.014 L/min
Voltage	[2.7–4.2] V	± (0.02% rdg. + 0.02% of FS)	± 0.00168 V
Current	[60–180] A	±0.05% of FS	± 0.05 A

References

[1] International Energy Agency, Global EV Outlook 2020, Glob. EV Outlook 2020, 2020.
[2] N. Priyadarshi, S. Padmanaban, R. Kumar, G. Amiya, R. Panda, R. Patel, Lecture Notes in Electrical Engineering 690 Advances in Power Systems and Energy Management Select Proceedings of ETAEERE 2020. 2020. <http://www.springer.com/series/7818>.
[3] M.F. Zia, E. Elbouchikhi, M. Benbouzid, Optimal operational planning of scalable DC microgrid with demand response, islanding, and battery degradation cost considerations, Appl. Energy 237 (January) (2019) 695–707.
[4] V.G. Choudhari, D.A.S. Dhoble, T.M. Sathe, A review on effect of heat generation and various thermal management systems for lithium ion battery used for electric vehicle, J. Energy Storage 32 (March) (2020) 101729.
[5] L. Lu, X. Han, J. Li, J. Hua, M. Ouyang, A review on the key issues for lithium-ion battery management in electric vehicles, J. Power Sources 226 (2013) 272–288.
[6] L.H. Saw, H.M. Poon, H.S. Thiam, Z. Cai, W.T. Chong, N.A. Pambudi, Y.J. King, Novel thermal management system using mist cooling for lithium-ion battery packs, Appl. Energy 223 (April) (2018) 146–158.
[7] J. Wang, P. Liu, J. Hicks-Garner, E. Sherman, S. Soukiazian, M. Verbrugge, H. Tataria, J. Musser, P. Finamore, Cycle-life model for graphite-LiFePO4 cells, J. Power Sources 196 (8) (2011) 3942–3948.
[8] P. Lyu, X. Liu, J. Qu, J. Zhao, Y. Huo, Z. Qu, Z. Rao, Recent advances of thermal safety of lithium ion battery for energy storage, Energy Storage Mater. 31 (March) (2020) 195–220.
[9] D. Ouyang, Y. He, J. Weng, J. Liu, M. Chen, J. Wang, Influence of low temperature conditions on lithium-ion batteries and the application of an insulation material, RSC Adv. 9 (16) (2019) 9053–9066.
[10] S. Ma, M. Jiang, P. Tao, C. Song, J. Wu, J. Wang, T. Deng, W. Shang, Temperature effect and thermal impact in lithium-ion batteries: a review, Prog. Nat. Sci. Mater. Int. 28 (6) (2018) 653–666.
[11] Q. Li, C. Yang, S. Santhanagopalan, K. Smith, J. Lamb, L.A. Steele, L. Torres-Castro, Numerical investigation of thermal runaway mitigation through a passive thermal management system, J. Power Sources 429 (2019) 80–88.
[12] M.S. Patil, J.H. Seo, S. Panchal, S.W. Jee, M.Y. Lee, Investigation on thermal performance of water-cooled Li-ion pouch cell and pack at high discharge rate with U-turn type microchannel cold plate, Int. J. Heat Mass Transf. 155 (2020) 119728.
[13] P. Kumar, D. Chaudhary, P. Varshney, U. Varshney, S.M. Yahya, Y. Rafat, Critical review on battery thermal management and role of nanomaterial in heat transfer enhancement for electrical vehicle application, J. Energy Storage 32 (October) (2020) 102003.
[14] M.K. Tran, S. Panchal, T.D. Khang, K. Panchal, R. Fraser, M. Fowler, Concept review of a cloud-based smart battery management system for lithium-ion batteries: feasibility, logistics, and functionality, Batteries 8(2) (2022).
[15] J. Kim, J. Oh, H. Lee, Review on battery thermal management system for electric vehicles, Appl. Therm. Eng. 149 (2019) 192–212.
[16] M. Al-Zareer, I. Dincer, M.A. Rosen, A review of novel thermal management systems for batteries, Int. J. Energy Res. 42 (10) (2018) 3182–3205.
[17] V.G. Choudhari, A.S. Dhoble, S. Panchal, M. Fowler, R. Fraser, Numerical investigation on thermal behaviour of 5 × 5 cell configured battery pack using phase change material and fin structure layout, J. Energy Storage 43 (November 2021) (2020) 103234.
[18] A.R.M. Siddique, S. Mahmud, B. Van Heyst, A comprehensive review on a passive (phase change materials) and an active (thermoelectric cooler) battery thermal management system and their limitations, J. Power Sources 401 (August) (2018) 224–237.
[19] H. Behi, D. Karimi, M. Behi, J. Jaguemont, M. Ghanbarpour, M. Behnia, M. Berecibar, J. Van Mierlo, Thermal management analysis using heat pipe in the high current discharging of lithium-ion battery in electric vehicles, J. Energy Storage 32 (September) (2020) 101893.
[20] C. Rouaud, Automotive Thermal Management (2020).
[21] X. Li, J. Zhao, J. Duan, S. Panchal, J. Yuan, R. Fraser, M. Fowler, M. Chen, Simulation of cooling plate effect on a battery module with different channel arrangement, J. Energy Storage 49 (January) (2022) 104113.
[22] Y. Chung, M.S. Kim, Thermal analysis and pack level design of battery thermal management system with liquid cooling for electric vehicles, Energy Convers. Manag. 196 (May) (2019) 105–116.
[23] C. Yang, L. Cao, The role of interfacial thermal resistance in Li-ion battery thermal management, ASME 2019 Int. Tech. Conf. Exhib. Packag. Integr. Electron. Photonic Microsystems, InterPACK 2019, no. February, 2019.
[24] 3M, Heat transfer applications using 3M ™ Novec ™ Engineered Fluids, 2015, pp. 1–2. <http://multimedia.3m.com/mws/media/1091997O/3m-novec-engineered-fluids-for-heat-transfer-line-card.pdf>.
[25] XING Mobility Dynamic Power on Demand, 2022. <https://www.xingmobility.com/assets/pdf/XingMobility_DynamicPower_OnDemand.pdf>.
[26] Kreisel Battery, Kreisel Battery Pack, 2022. <https://www.kreiselelectric.com/>.
[27] S. Park, D. Jung, Battery cell arrangement and heat transfer fluid effects on the parasitic power consumption and the cell temperature distribution in a hybrid electric vehicle, J. Power Sources 227 (2013) 191–198.
[28] D.W. Sundin, S. Sponholtz, Thermal management of li-ion batteries with single-phase liquid immersion cooling, IEEE Open J. Veh. Technol. 1 (2020) 82–92.
[29] G. Pulugundla, P. Dubey, Z. Wu, Q. Wang, A. K. Srouji, Thermal management of lithium ion cells at high discharge rate using submerged-cell cooling, in: 2020 IEEE Transp. Electrif. Conf. Expo, ITEC 2020, 2020.
[30] P. Dubey, G. Pulugundla, A.K. Srouji, Direct comparison of immersion and cold-plate based cooling for automotive li-ion battery modules, Energies 14(5) (2021).
[31] S. Wu, L. Lao, L. Wu, L. Liu, C. Lin, Q. Zhang, Effect analysis on integration efficiency and safety performance of a battery thermal management system based on direct contact liquid cooling, Appl. Therm. Eng. 201 (PA) (2022) 117788.
[32] M. Suresh Patil, J.H. Seo, M.Y. Lee, A novel dielectric fluid immersion cooling technology for Li-ion battery thermal management, Energy Convers. Manag. 229 (September 2020) (2021) 113715.
[33] M. Li, J. Wang, Q. Guo, Y. Li, Q. Xue, G. Qin, Numerical analysis of cooling plates with different structures for electric vehicle battery thermal management systems, J. Energy Eng. 146 (4) (2020) 1–10.
[34] T. Amalesh, N.L. Narasimhan, Introducing new designs of minichannel cold plates for the cooling of Lithium-ion batteries, J. Power Sources 479 (July) (2020) 228775.
[35] G.O. Brown, The history of the Darcy-Weisbach equation for pipe flow resistance, Proc. Environ. Water Resour. Hist. 40650 (January) (2002) 34–43.